The Enok acetyltransferase complex interacts with Elg1 and negatively regulates PCNA unloading to promote the G1/S transition

Fu Huang,[1,2] Anita Saraf,[1] Laurence Florens,[1] Thomas Kusch,[3] Selene K. Swanson,[1] Leanne T. Szerszen,[1] Ge Li,[1] Arnob Dutta,[1] Michael P. Washburn,[1,4] Susan M. Abmayr,[1,5] and Jerry L. Workman[1]

[1]Stowers Institute for Medical Research, Kansas City, Missouri 64110, USA; [2]Institute of Biological Chemistry, Academia Sinica, Taipei 11529, Taiwan; [3]Department of Molecular Biology and Biochemistry, Rutgers, The State University of New Jersey, Piscataway, New Jersey 08854, USA; [4]Pathology and Laboratory Medicine, University of Kansas Medical Center, Kansas City, Kansas 66160, USA; [5]Department of Anatomy and Cell Biology, University of Kansas Medical Center, Kansas City, Kansas 66160, USA

KAT6 histone acetyltransferases (HATs) are highly conserved in eukaryotes and are involved in cell cycle regulation. However, information regarding their roles in regulating cell cycle progression is limited. Here, we report the identification of subunits of the *Drosophila* Enok complex and demonstrate that all subunits are important for its HAT activity. We further report a novel interaction between the Enok complex and the Elg1 proliferating cell nuclear antigen (PCNA)-unloader complex. Depletion of Enok in S2 cells resulted in a G1/S cell cycle block, and this block can be partially relieved by depleting Elg1. Furthermore, depletion of Enok reduced the chromatin-bound levels of PCNA in both S2 cells and early embryos, suggesting that the Enok complex may interact with the Elg1 complex and downregulate its PCNA-unloading function to promote the G1/S transition. Supporting this hypothesis, depletion of Enok also partially rescued the endoreplication defects in Elg1-depleted nurse cells. Taken together, our study provides novel insights into the roles of KAT6 HATs in cell cycle regulation through modulating PCNA levels on chromatin.

In eukaryotes, proliferating cell nuclear antigen (PCNA) forms a ring-shaped homotrimer and plays crucial roles in DNA replication and repair. PCNA functions as a sliding clamp that enhances the processivity of DNA polymerases and recruits other proteins to facilitate DNA replication (Moldovan et al. 2007). The PCNA homotrimer is loaded onto DNA at template–primer junctions by the replication factor C (RFC) complex in an ATP-dependent manner (Majka and Burgers 2004). Once PCNA is loaded, replicative DNA polymerase δ (Pol δ) or Pol ε associates with PCNA and carries out DNA synthesis on lagging and leading strands, respectively (Garg et al. 2004). After the completion of DNA synthesis and Okazaki fragment maturation, the Elg1 RFC-like complex has recently been reported to unload PCNA from DNA (Kubota et al. 2013, 2015).

The pentameric RFC complex is composed of one large subunit (Rfc1) and four small subunits (Rfc2–5). In addi-

tion to the RFC complex, three RFC-like complexes have been identified in yeast. These RFC-like complexes share the four small subunits with the RFC complex, but each of them contains an alternative large subunit in place of Rfc1: Elg1, Ctf18, or Rad24 (Kim and MacNeill 2003). Elg1 is important for maintaining genome stability and plays a role in sister chromatid cohesion (Bellaoui et al. 2003; Ben-Aroya et al. 2003; Kanellis et al. 2003; Parnas et al. 2009). Recently, the Elg1 complex has been characterized as the PCNA unloader during DNA replication (Kubota et al. 2013). The PCNA-unloading function of Elg1 is likely conserved in mammals, as depleting the human homolog of Elg1, ATAD5, in cultured cells resulted in the accumulation of PCNA on chromatin (Lee et al. 2013). In addition, human ATAD5 interacts with the deubiquitinase USP1 and facilitates PCNA

deubiquitination by USP1, suggesting a possible involvement of ATAD5 in the response to DNA damage (Sikdar et al. 2009; Lee et al. 2010). In *Drosophila*, the Elg1 homolog has been recently identified in a large-scale screen and reported to be critical for proper development of the female germline (Hayashi et al. 2014). While the functions of Elg1/ATAD5 have been revealed at the molecular level and in development, information regarding regulation of the Elg1 complex as a PCNA unloader is still lacking.

The KAT6 histone acetyltransferases (HATs) are highly conserved in a wide range of eukaryotes and preferentially acetylate histone H3 in nucleosomes (John et al. 2000; Ullah et al. 2008; Huang et al. 2014). Notably, increasing evidence suggests their involvement in cell cycle regulation. The yeast KAT6 Sas3 has been shown to play a role in gene silencing and cell cycle progression (Howe et al. 2001), and its mammalian homolog, MOZ, was first identified as a fusion partner of CBP in acute myeloid leukemia (AML) (Yang and Ullah 2007). In addition, MOZ has been shown to promote the expression of p21 by interacting with p53 (Rokudai et al. 2013) and is required for the proliferation of hematopoietic precursors (Perez-Campo et al. 2009). In *Drosophila*, the KAT6 Enok is important for neuroblast proliferation and therefore is required for mushroom body development (Scott et al. 2001). However, the molecular mechanisms underlying its roles in regulating cell proliferation remain unclear. In this study, we characterized the composition of the Enok complex and identified the Elg1 complex as a novel interacting partner. Depletion of Enok resulted in an Elg1-dependent block at the G1/S transition and reduced chromatin-bound PCNA levels. Furthermore, knocking down *enok* partially rescued the defective nurse cell endoreplication observed in the Elg1-depleted germline. Therefore, our results suggest that Enok may down-regulate PCNA unloading from DNA by interacting with the Elg1 complex and may promote the G1/S transition of the cell cycle.

Results

Enok activity in vivo requires Br140, Eaf6, and Ing5

While the composition of complexes formed by the human and yeast KAT6 has been characterized (Doyon et al. 2006; Taverna et al. 2006; Gilbert et al. 2014), information regarding the *Drosophila* Enok complex is lacking. We sought to identify core components of the Enok complex and assess their roles in mediating the HAT function of this complex. To this end, the Enok complex was isolated using Flag affinity purification from S2 cell nuclear extracts (NEs) with Flag-tagged Enok as the bait protein, and the composition of purified complex was determined by multidimensional protein identification technology (MudPIT) (Florens and Washburn 2006). Peptides from the *Drosophila* homologs of three subunits in the human MOZ/MORF complexes were identified: Br140, Eaf6, and CG9293 (Fig. 1A). Furthermore, MudPIT analysis of Flag affinity-purified complexes using Br140, Eaf6, or CG9293 as the bait protein consistently identified peptides from Enok, Br140, Eaf6, and CG9293 (Fig. 1A). These results indicate that the Enok complex is composed of these four proteins and is homologous to the human MOZ/MORF complex. Based on the conserved composition of the Enok complex and the specific sequence similarity between CG9293 and human ING5, CG9293 is referred to here as Ing5.

We next asked whether the subunits of the Enok complex are important for its in vivo HAT function. We previously reported that Enok functions as the major HAT for establishing the H3K23ac mark in flies (Huang et al. 2014) and therefore used the global H3K23ac levels as a monitor for the HAT function of the complex. Each of the four subunits was depleted in S2 cells using dsRNAs against the corresponding genes, and the levels of H3K23ac and H3K14ac were examined by Western blotting. RT-qPCR analysis showed that treatment of each dsRNA resulted in 60%–85% reduction specifically in mRNA levels of the target gene, and mRNA levels of the other three genes were largely unaffected compared with the control LacZ dsRNA treatment (Fig. 1B, right panel). Depletion of any of the four subunits led to reductions in the H3K23ac levels without affecting the H3K14ac levels (Fig. 1B, left panel, lanes 2–5), indicating that all four components are important for the full HAT function of the Enok complex in vivo. Interestingly, Enok protein levels were decreased in the Br140-depleted cells (Fig. 1B, left panel, lane 3), suggesting that Br140 may also play a role in maintaining the protein levels/stability of Enok. To further examine whether Br140 can stimulate the HAT activity of Enok, we performed an in vitro HAT assay with recombinant Enok and Br140 purified using the baculovirus expression system. Indeed, the HAT activity of Enok toward either short oligonucleosomes from HeLa cells (Fig. 1C) or recombinant nucleosomes (Fig. 1D) was higher in the presence of Br140 (Fig. 1D, cf. lanes 2 and 4). In addition, Enok alone failed to acetylate H3K14 as we reported previously (Huang et al. 2014), but, in the presence of Br140, Enok showed HAT activity toward H3K14 (Fig. 1D, lane 4). This result suggests that Br140 may also regulate the substrate specificity of Enok. Taken together with the in vivo data shown in Figure 1B, we concluded that all four subunits are important for full HAT activity of the Enok complex.

The Enok complex interacts with the Elg1 PCNA-unloader complex

Intriguingly, the above-mentioned MudPIT analysis of Br140 purification identified peptides from all components of the Elg1 PCNA-unloader complex: Elg1, Rfc4, Rfc38, CG8142, and Rfc3 (Fig. 2A). Affinity purification of Elg1 also reciprocally copurified the entire Enok complex (Fig. 2A). These results suggested that the Enok complex may interact with the Elg1 complex in vivo. However, only Elg1 was identified in the affinity purification of Enok (Fig. 2A), probably due to the low yield of purification resulting from intrinsic properties of Enok that include instability and inefficient elution. Based on the conserved composition of the Elg1 complex and the
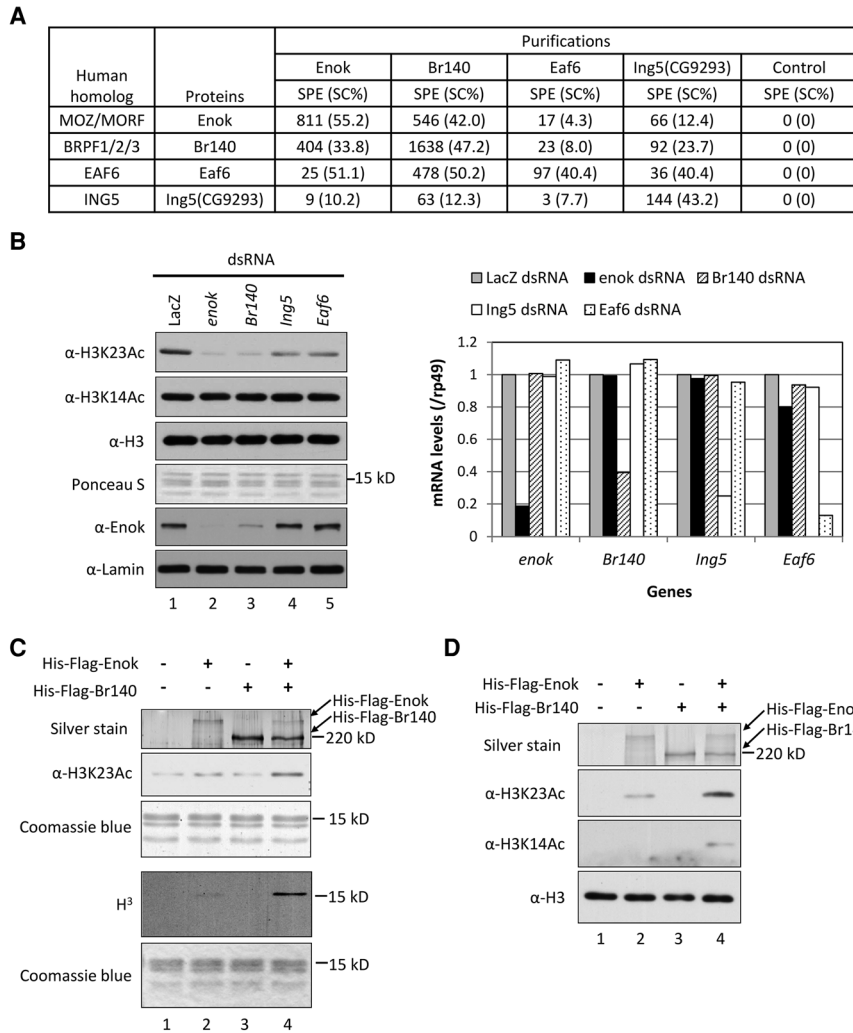
A

Human homolog	Proteins	Purifications				
		Enok	Br140	Eaf6	Ing5(CG9293)	Control
		SPE (SC%)	SPE (SC%)	SPE (SC%)	SPE (SC%)	SPE (SC%)
MOZ/MORF	Enok	811 (55.2)	546 (42.0)	17 (4.3)	66 (12.4)	0 (0)
BRPF1/2/3	Br140	404 (33.8)	1638 (47.2)	23 (8.0)	92 (23.7)	0 (0)
EAF6	Eaf6	25 (51.1)	478 (50.2)	97 (40.4)	36 (40.4)	0 (0)
ING5	Ing5(CG9293)	9 (10.2)	63 (12.3)	3 (7.7)	144 (43.2)	0 (0)

B

C

D

Figure 1. Enok forms a quartet complex homologous to the human MOZ complex. (A) MudPIT analysis of Flag affinity purifications of Flag-HA-tagged Enok, Br140, Eaf6, and Ing5 showed copurification of these four components. Parental S2 cells were used in mock purification as a control. (SPE) Spectral count; (SC%) sequence coverage (percentage). (B) S2 cells were treated with control dsRNA (LacZ) or dsRNAs against subunits of the Enok complex and subjected to RT-qPCR analysis (right panel), acid extraction of histones (top left four panels), and nuclear extraction (bottom left two panels) followed by Western blotting. (C,D) In vitro HAT assay was performed using recombinant His-Flag-tagged Enok and Br140. Substrates were short oligonucleosomes from HeLa cells (C) or nucleosomes reconstituted using 601 positioning sequence and recombinant histones (D).

sequence similarity between CG8142 and human RFC4/RFC37, we refer to CG8142 here as Rfc37.

To confirm the in vivo interaction between Enok and Elg1, coimmunoprecipitation (co-IP) was performed in S2 cells using Enok- or Elg1-specific antibodies (Supplemental Fig. S1; Huang et al. 2014). Consistent with the MudPIT analysis, both endogenous Enok and Elg1 were immunoprecipitated by the α-Enok antibody, and the immunoprecipitation of Elg1 was dependent on the presence of Enok protein (Fig. 2B, left panel, lanes 2,3). Also, endogenous Enok was specifically immunoprecipitated by the α-Elg1 antibody but not by the preimmune serum (Fig. 2B, right panel, lanes 6,7), indicating that Enok indeed interacts with Elg1 in vivo.

We further examined whether these two complexes interact directly with each other. To this end, in vitro pull-down assays were performed using the baculovirus expression system. As shown in Figure 2C, pulling down Elg1 through its HA tag also pulled down Br140 but not Enok (left panel, lanes 4,5). Consistently, when Enok or Br140 was pulled down through its Flag tag, Elg1 was only pulled down with Br140 (Fig. 2C, middle panel, lanes 6–8). However, in the presence of no-tag Br140, Elg1 was

pulled down with the Flag-tagged Enok (Fig. 2C, middle panel, lane 9). Taken together, results from our MudPIT analysis and pull-down assays suggested that Br140 serves as the bridge between the Enok and Elg1 complexes (Fig. 2C, right panel).

The G1/S block in Enok-depleted cells is partially dependent on Elg1

The Elg1 complex was recently reported as the PCNA unloader in yeast and human cells (Kubota et al. 2013; Lee et al. 2013). The human homolog of Elg1, ATAD5, has also been shown to facilitate PCNA deubiquitination (Lee et al. 2010). In S2 cells, knocking down *elg1* using dsRNAs did not affect total PCNA levels but resulted in increases in the levels of both chromatin-bound PCNA and monoubiquitinated PCNA (PCNAub) (Supplemental Fig. S2A), suggesting that the functions of Elg1 in unloading and deubiquitination of PCNA are conserved in flies.

To investigate the functional link between the Enok and the Elg1 complexes, we first asked whether the Elg1 complex is involved in regulating the HAT function of the Enok complex. While depletion of Enok reduced the
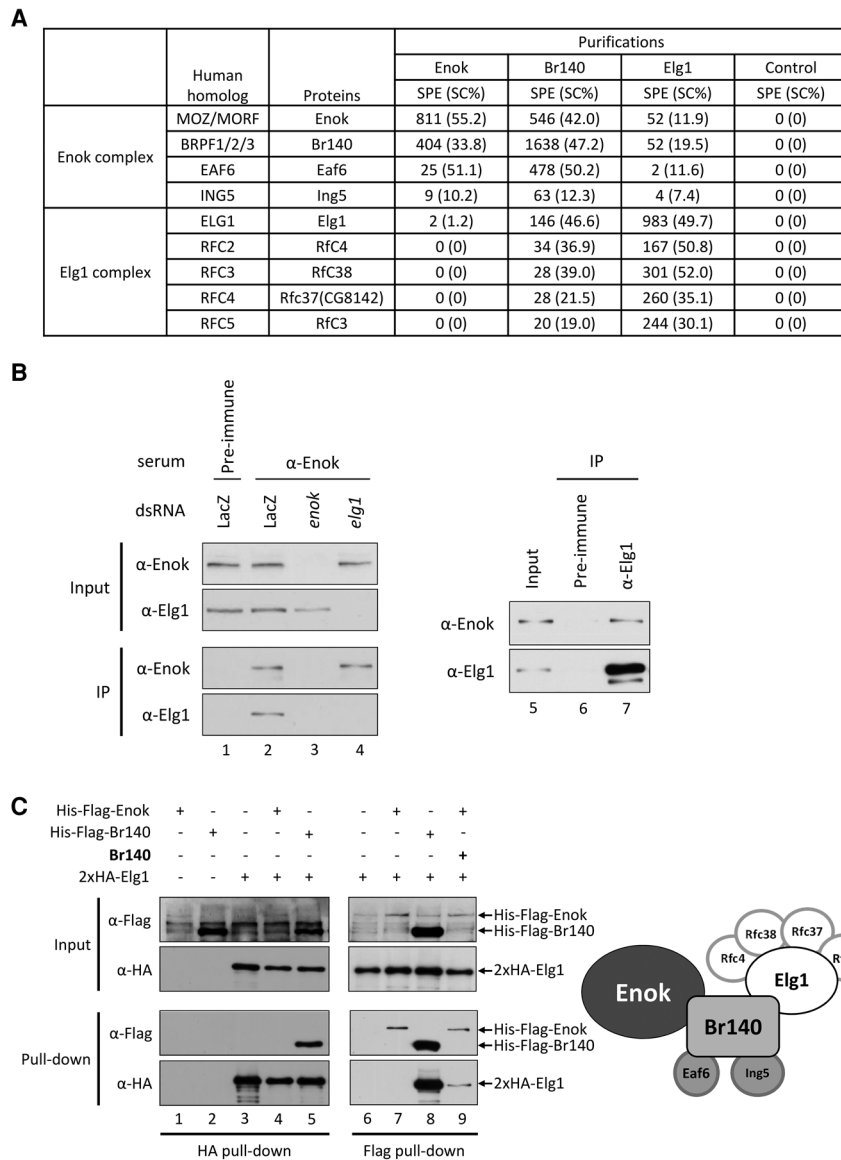
A

		Purifications			
Human homolog	Proteins	Enok SPE (SC%)	Br140 SPE (SC%)	Elg1 SPE (SC%)	Control SPE (SC%)
Enok complex					
MOZ/MORF	Enok	811 (55.2)	546 (42.0)	52 (11.9)	0 (0)
BRPF1/2/3	Br140	404 (33.8)	1638 (47.2)	52 (19.5)	0 (0)
EAF6	Eaf6	25 (51.1)	478 (50.2)	2 (11.6)	0 (0)
ING5	Ing5	9 (10.2)	63 (12.3)	4 (7.4)	0 (0)
Elg1 complex					
ELG1	Elg1	2 (1.2)	146 (46.6)	983 (49.7)	0 (0)
RFC2	RfC4	0 (0)	34 (36.9)	167 (50.8)	0 (0)
RFC3	RfC38	0 (0)	28 (39.0)	301 (52.0)	0 (0)
RFC4	Rfc37(CG8142)	0 (0)	28 (21.5)	260 (35.1)	0 (0)
RFC5	RfC3	0 (0)	20 (19.0)	244 (30.1)	0 (0)

B

C

Figure 2. The Enok complex interacts with the Elg1 complex. (*A*) MudPIT analysis of Flag affinity purifications of Flag-HA-tagged Enok, Br140, and Elg1 showed co-purification of the Enok complex and the Elg1 complex. Parental S2 cells were used in mock purification as a control. (SPE) Spectral count; (SC%) sequence coverage (percentage). (*B*) Interaction between endogenous Enok and Elg1 in S2 cells was examined by coimmunoprecipitation (co-IP). (*Left* panel) Four percent of NEs from S2 cells treated with LacZ dsRNA (control) or dsRNA against *enok* or *elg1* were used as input. Rabbit α-Enok serum and protein A-conjugated resin were used to immunoprecipitate endogenous Enok, and the corresponding preimmune serum was used as a control. Input and 30% of immunoprecipitates were subjected to Western blot analysis using guinea pig α-Enok and α-Elg1 antibodies. (*Right* panel) Four percent of the NE from S2 cells were used as input. Rabbit α-Elg1 serum and protein A-conjugated resin were used to immunoprecipitate endogenous Elg1, and the corresponding preimmune serum was used as a control. Input and 50% of immunoprecipitates were subjected to Western blotting using guinea pig α-Enok and α-Elg1 antibodies. (*C*) Br140 directly interacts with Elg1 in vitro. Recombinant 2xHA-Elg1, His-Flag-Enok, His-Flag-Br140, or no-tag Br140 was expressed in Sf9 cells using the baculovirus system. (*Left* panel) Of the whole-cell lysates from Sf9 cells expressing the indicated recombinant proteins, 3.75% (α-Flag) and 1.25% (α-HA) were used as input. Anti-HA antibody-conjugated resin was used to pull down HA-tagged Elg1. Input and 85% (α-Flag)/15% (α-HA) of pull-down were subjected to Western blot analysis. (*Middle* panel) Five percent (α-Flag) and 1% (α-HA) of whole-cell lysates from Sf9 cells expressing the indicated recombinant proteins were used as input. Anti-Flag antibody-conjugated resin was used to pull down Flag-His-Enok or Flag-His-Br140. Input and 40% (α-Flag)/50% (α-HA) of pull-down were subjected to Western blot analysis. (*Right* panel) A schematic representation of the interaction between the Enok and Elg1 complexes.

global level of H3K23ac in S2 cells, depletion of either Elg1 or Rfc4 had no obvious effect on levels of this histone mark (Supplemental Fig. S2B). Also, the H3K23ac levels in third instar larvae were largely unaffected in a mutant lacking functional Elg1 as compared with the heterozygote control (Supplemental Fig. S6B). Therefore, the Elg1 complex may not significantly contribute to the establishment of H3K23ac by the Enok complex. Since Elg1 has been reported to play a role in maintaining genome stability in yeast (Bellaoui et al. 2003; Ben-Aroya et al. 2003; Kanellis et al. 2003), we examined the γH2Av levels in the Enok- and/or Elg1-depleted S2 cells to assess DNA damage levels. As shown in Supplemental Figure S2C, the γH2Av levels were not increased in S2 cells upon depletion of Enok or Elg1, suggesting that the genome stability in S2 cells may be less sensitive to reduced Elg1 levels than in yeast. We next asked whether Enok plays a role in cell cycle regulation through interaction with the Elg1 complex. Knocking down *enok* in S2 cells resulted in an accumulation of cells in the G1 phase compared with control cells treated with LacZ dsRNA (Fig. 3A). Interestingly, knocking down *elg1* in Enok-depleted cells (*enok+elg1* dsRNA) partially rescued the G1 accumulation phenotype compared with *enok* dsRNA alone (Fig. 3A), and this rescuing effect was not due to differences in knockdown efficiencies (Fig. 3B,C).

Since depletion of Enok did not significantly affect the S-phase progression in S2 cells (Supplemental Fig. S3),
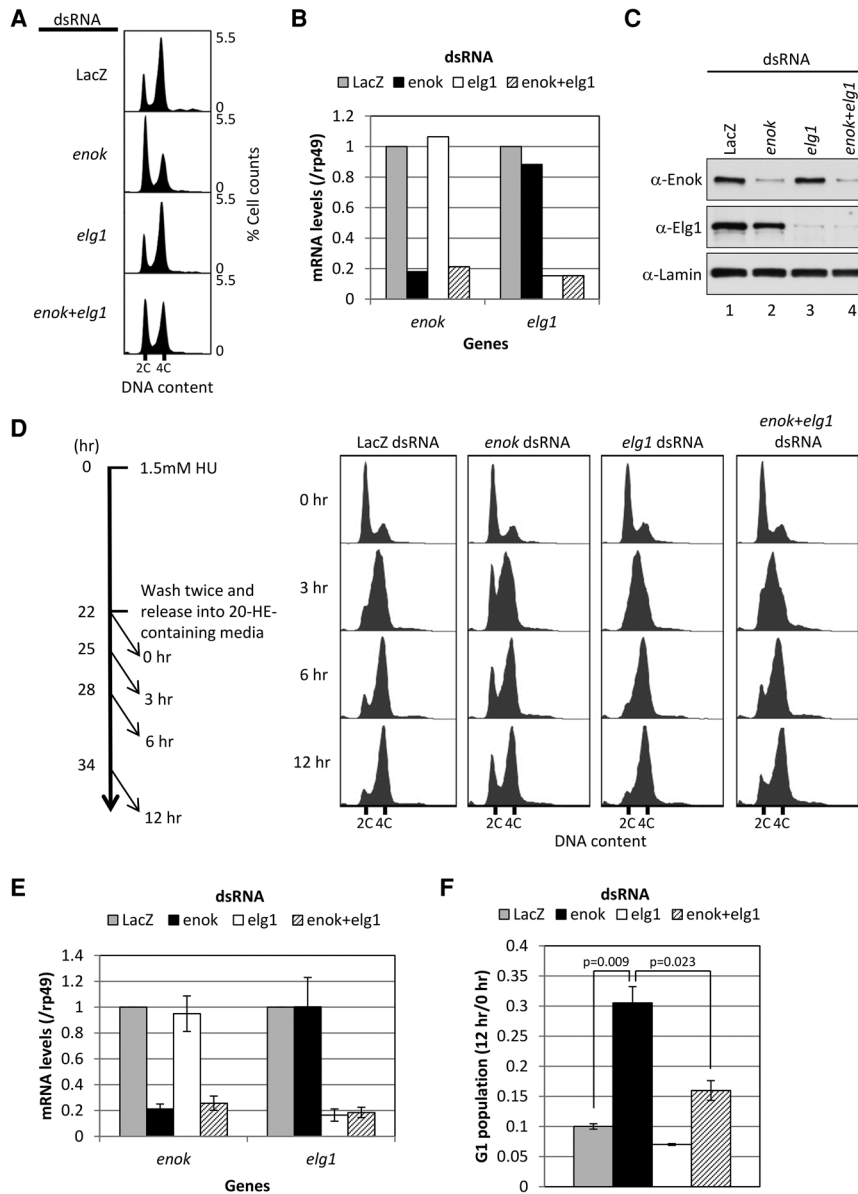
Figure 3. Depletion of Elg1 partially rescues the G1/S block in Enok-depleted cells. (*A*) Flow cytometric analysis of S2 cells treated with LacZ dsRNA or dsRNA against *enok* and/or *elg1*. (*B*) The expression levels of *enok* and *elg1* were examined by RT-qPCR in the S2 cells treated with LacZ dsRNA (control) or dsRNAs against *enok* and/or *elg1*. The mRNA levels of *enok* and *elg1* were normalized to the levels of *rp49*. (*C*) NEs of S2 cells treated with LacZ dsRNA or dsRNAs against *enok* and/or *elg1* were subjected to Western blot analysis using α-Enok and α-Elg1 antibodies. Lamin was used as the loading control. (*D*–*F*) S2 cells treated with dsRNAs against the indicated genes were first arrested at the G1/S transition by 1.5 mM hydroxyurea (HU) and were released into fresh medium containing 1.7 μM 20-hydroxyecdysone (20-HE), which would further arrest S2 cells at the G2/M phase, to prevent S2 cells from re-entering the G1 phase. Cells were then removed from culture at the indicated time points and subjected to flow cytometric analysis (*D*) and RT-qPCR analysis (*E*). Percentages of cells in the G1 phase were calculated using the ModFit software, and the ratios of G1 population at 12 h to that at 0 h were shown in *F*. In *E* and *F*, data represent the mean of two biological replicates ± SD.

we reasoned that the G1 accumulation phenotype of Enok-depleted cells may result from an increased G2/M progression rate and/or a block at the G1/S transition. Therefore, we examined G2/M progression in S2 cells by labeling the S-phase population with bromodeoxyuridine (BrdU) and following the progression of BrdU-positive cells from G2/M to G1. Indeed, depletion of Enok in S2 cells led to an increased rate of G2/M progression compared with control cells treated with LacZ dsRNA (Supplemental Fig. S4). However, knocking down *elg1* in Enok-depleted cells (*enok+elg1* dsRNA) did not rescue the G2/M progression phenotype compared with cells treated with *enok* dsRNA only (Supplemental Figs. S4C–E). While the increased rate of G2/M progression in Enok-depleted cells is not dependent on Elg1, this phenotype suggests that Enok may negatively regulate the progression from G2/M to G1 in the cell cycle.

We next examined G1/S progression in dsRNA-treated S2 cells. The S2 cells were first arrested at the G1/S transition using hydroxyurea (HU) and then were released into medium containing 20-hydroxyecdysone (20-HE). This treatment further arrested S2 cells at the G2/M phase and prevented cells from re-entering the G1 phase (Fig. 3D, left panel; MacAlpine et al. 2004). Cell cycle profile analysis following release from HU showed that knocking down *enok* in S2 cells resulted in a G1/S block as compared with the cells treated with control LacZ dsRNA (Fig. 3D–F). Furthermore, depletion of Elg1 partially relieved the G1/S block in Enok-depleted cells. As shown in Figure 3F, the ratio of G1 cells in the population at 12 h compared with 0 h in the *enok* dsRNA-treated cells (31%) was threefold higher than the 10% ratio in control cells treated with LacZ dsRNA. However, this ratio was decreased to 16% in the *enok+elg1* dsRNA-treated cells.

Since knocking down *elg1* in Enok-depleted cells brought this 12/0 h ratio much closer to the 10% observed in control cells, we concluded that Enok plays a role that is partially dependent on Elg1 in regulating the G1/S transition.

Enok is important for maintaining the level of chromatin-bound PCNA

Given that the Elg1 complex functions as the PCNA unloader and that depletion of PCNA led to an increase in the population of cells in G1 (Supplemental Figs. S5A, B), the functional interaction between Enok and Elg1 at the G1/S transition prompted us to examine by cell fractionation analysis whether Enok is involved in regulating PCNA levels on chromatin. Indeed, knocking down *enok* in asynchronous S2 cells led to reduced PCNA levels in the chromatin fraction without affecting the total PCNA levels as compared with cells treated with the control LacZ dsRNA (Fig. 4A, lanes 1,2). In addition, knocking down *enok* in Elg1-depleted cells also reduced the levels of PCNA in the chromatin fraction (Fig. 4A, lanes 3,4), suggesting that Enok may negatively regulate the PCNA-unloading functions of Elg1. The reduction in chromatin-bound PCNA levels in Enok-depleted cells is unlikely due to the accumulation of cells in G1 (Fig. 3A), as chromatin-bound PCNA levels are higher at the G1/S transition than in other cell cycle phases (Supplemental Fig.

S2A, lanes 1,3,5,7). In addition, upon *enok* dsRNA treatment, we observed a similar reduction in chromatin-bound PCNA levels accompanied by an increase in cytosolic PCNA levels in S2 cells synchronized at the G1/S transition (Supplemental Figs. S5C,D, cf. lanes 4,5 and 10,11). This result further confirms a role for Enok in maintaining PCNA levels on chromatin.

We next asked whether Enok has a similar role in regulating chromatin-bound PCNA levels in flies. RNAi against *enok* in early embryos was carried out using a *UAS-shRNA-enok* transgene driven by MTD-Gal4 (Ni et al. 2011). In 0- to 3-h embryos, knocking down *enok* decreased PCNA levels in the chromatin-enriched fraction without affecting global PCNA levels as compared with control embryos from *MTD-Gal4/UAS-Luciferase* females (Fig. 4B, lanes 3,4). Therefore, taken together with the physical and functional interactions between Enok and Elg1 (Figs. 2, 3), we hypothesized that the Enok complex may associate with the Elg1 complex and down-regulate its PCNA-unloading function to promote the G1/S transition (Fig. 4C).

enok *genetically interacts with* elg1 *in the female germline*

To further test our hypothesis, we sought to examine the genetic interaction between *enok* and *elg1* in flies. The
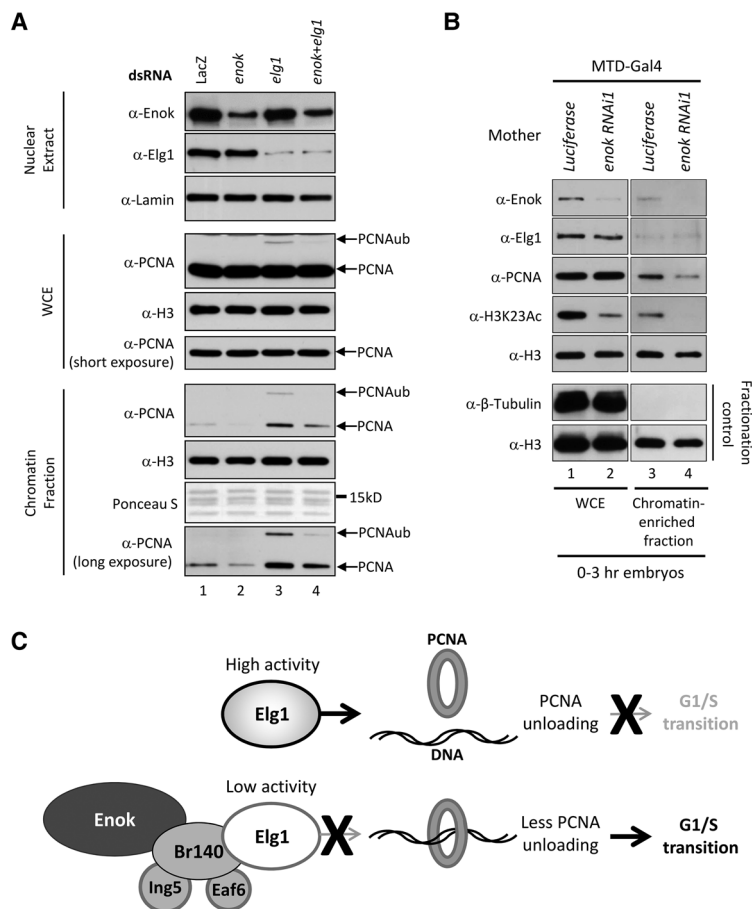

Figure 4. Depletion of Enok reduces the levels of chromatin-bound PCNA. (*A*) S2 cells treated with LacZ dsRNA (control) or dsRNAs against the indicated genes were subjected to a preparation of NEs, whole-cell extracts (WCEs), or chromatin fractions followed by Western blot analysis. Lamin, Histone H3, and Ponceau S staining were used as loading controls. (*B*) WCEs and chromatin-enriched fractions were prepared from 0- to 3-h embryos and subjected to Western blotting. The *bottom* two panels show images with the same exposure time from the same blot probed with α-β-Tubulin and α-H3 antibodies, respectively, as the fractionation controls. The genotypes of the mothers used were as follows: *P{w[+mC]=otu-GAL4::VP16.R}1/+; P{w[+mC]=GAL4-nos. NGT}40/+; P{w[+mC]=GAL4::VP16-nos.UTR}CG6325 MVD1/P{y[+t7.7] v[+t1.8]=UAS-LUC.VALIUM10}attP2* (*Luciferase*) and *P{w[+mC]=otu-GAL4::VP16.R}1/+; P{w [+mC]=GAL4-nos. NGT}40/+; P{w[+mC]=GAL4::VP16-nos.UTR}CG6325MVD1/P{TRiP.HMS02165}attP2* (*enok RNAi1*). (*C*) Schematic representation of the proposed model. The Enok complex interacts with Elg1 through Br140, inhibits the PCNA-unloading function of Elg1, and therefore promotes the G1/S transition.

$elg1^{MI08386}$ allele contains a 7.3-kb P-element insertion inside the coding region of the ATPase domain in Elg1 (Venken et al. 2011). This insert severely reduced the level of full-length Elg1 in NEs from $elg1^{MI08386}$ ovaries as compared with yw ovaries (Supplemental Fig. S6A). Interestingly, the $elg1^{MI08386}$ mutant is viable, but the females fail to generate mature eggs. Consistent with a recent study reporting that another $elg1$ mutant ($elg1^{3R7}$) showed apparently underreplicated nurse cell nuclei (Hayashi et al. 2014), nurse cell nuclei in $elg1^{MI08386}$ ovaries also showed an underreplicated morphology (Supplemental Fig. S6C). The fertility and nurse cell morphology of $elg1^{MI08386}$ mutant females was not complemented by $Df(3L)Exel6128$, a chromosomal deletion eliminating the entire $elg1$ gene (Supplemental Fig. S6D). Moreover, MTD-Gal4-driven RNAi against $elg1$ in the female germline phenocopied the $elg1$ mutant phenotype in nurse cells (Fig. 5B; Supplemental Fig. S8A). Since the DNA damage levels assessed by γH2Av staining were not elevated in $elg1^{MI08386}$ nurse cells as compared with the yw

control (Supplemental Fig. S6E), we reasoned that Elg1 is important for proper nurse cell endoreplication. Therefore, we examined the DNA replication pattern in nurse cells by BrdU labeling. Indeed, while the heterochromatic regions in nurse cell nuclei were normally underreplicated during endoreplication after stage 5 in the yw control (Royzman et al. 2002), heterochromatin in the $elg1^{MI08386}$ nurse cells was still actively replicated (Supplemental Fig. S6F, white arrowheads), confirming that disruption of Elg1 function resulted in defects in nurse cell endoreplication. The phenotype of overreplication of heterochromatin in the $elg1^{MI08386}$ nurse cells is similar to that observed in the $cyclin E$ ($cycE$) mutant and the Cyclin E/Cdk2 inhibitor $dacapo$ (dap) mutant (Lilly and Spradling 1996; Hong et al. 2007). These $cycE$ and dap mutant phenotypes were suggested to result from a prolonged S phase during nurse cell endocycles. A similar phenotype might result from compromising the function of Elg1, leading to inefficient PCNA unloading and an extended endocycle S phase. In addition, although we did not observe
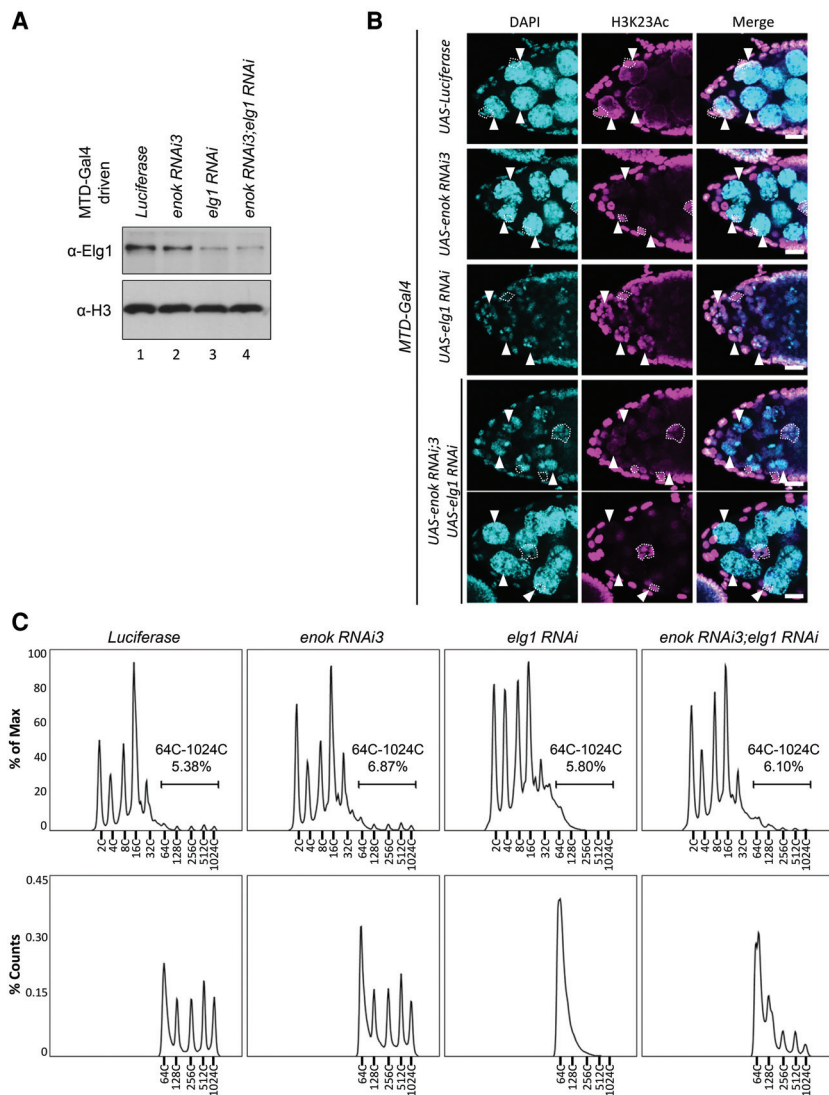

Figure 5. Genetic interaction between $enok$ and $elg1$. (A) Chromatin-enriched fractions were prepared from ovaries and subjected to Western blotting. Histone H3 was used as the loading control. (B) Stage 9 egg chambers were stained with DAPI and an α-H3K23ac antibody. White dashed lines depict somatic border/follicle cells overlapping with nurse cells in the images. White arrowheads indicate nurse cells for comparison between samples. Posterior is to the right. Bars, 20 µm. (C) Ovaries were subjected to flow cytometric analysis. (*Top* panel) Histograms of cells with a ploidy level of 2C–1024C. (*Bottom* panel) Histograms of nurse cells with a ploidy level of 64C–1024C. In A–C, the genotypes of the females used were as follows: $P\{w[+mC]=otu-GAL4::VP16.R\}1/+$; $P\{w[+mC]=GAL4-nos.NGT\}40/+$; $P\{w[+mC]=GAL4::VP16-nos.UTR\}CG6325MVD1/P\{y[+t7.7] v[+t1.8]=UAS-LUC.VALIUM10\}attP2$ (*Luciferase*), $P\{w[+mC]=otu-GAL4::VP16.R\}1/+$; $P\{w[+mC]=GAL4-nos.NGT\}40/P\{TRiP.HMS02165\}attP40$; $P\{w[+mC]=GAL4::VP16-nos.UTR\}CG6325MVD1/+$ (*enok RNAi3*), $P\{w[+mC]=otu-GAL4::VP16.R\}1/+$; $P\{w[+mC]=GAL4-nos.NGT\}40/+$; $P\{w[+mC]=GAL4::VP16-nos.UTR\}CG6325MVD1/P\{TRiP.HMC03187\}attP2$ (*elg1 RNAi*), and $P\{w[+mC]=otu-GAL4::VP16.R\}1/+$; $P\{w[+mC]=GAL4-nos.NGT\}40/P\{TRiP.HMS02165\}attP40$; $P\{w[+mC]=GAL4::VP16-nos.UTR\}CG6325MVD1/P\{TRiP.HMC03187\}attP2$ (*enok RNAi3;elg1 RNAi*).

increased levels of γH2Av in *elg1*[MI08386] ovaries (Supplemental Fig. S6E), we cannot exclude the possibility that Elg1 is important for the DNA damage signaling pathway that leads to establishment of the γH2Av mark.

We reasoned that if Enok negatively regulates the PCNA-unloading function of Elg1, then knocking down *enok* in the female germline may partially rescue the endoreplication defects in Elg1-depleted nurse cells by increasing the activity of residual Elg1. To test this hypothesis, RNAi against *enok* and/or *elg1* in the female germline was carried out using *UAS-shRNA-enok* and *UAS-shRNA-elg1* transgenes driven by MTD-Gal4. To confirm the specificity of RNAi against *enok*, we examined two different *enok RNAi* transgenes: *enok RNAi2* (Supplemental Figs. S7–S9) and *enok RNAi3* (Fig. 5). Because both the *UAS-enok RNAi1* (Fig. 4B) and the *UAS-elg1 RNAi* fly lines contain the RNAi transgene in the *attP2* site, we obtained the *UAS-enok RNAi2* line containing a different shRNA construct against *enok* in the *attP40* site from the Bloomington *Drosophila* Stock Center. We also generated the *UAS-enok RNAi3* line that has the same shRNA construct against *enok* as the *UAS-enok RNAi1* line in the *attP40* site (see the Materials and Methods for details). As shown by the expression of *EGFP* from a gene trap cassette in the *elg1*[MI08386] allele, *elg1* is expressed at higher levels in the germline nurse cells than in the somatic follicle cells (Supplemental Fig. S7A). A reduction in Elg1 protein levels was therefore visible by Western blotting when *elg1 RNAi* was driven in the germline by MTD-Gal4 and confirmed that Elg1 protein levels were similar in the *elg1 RNAi* and the double RNAi (*enok RNAi+elg1 RNAi*) ovaries (Fig. 5A; Supplemental Fig. S7B). However, the levels of the enzymatic product of Enok (H3K23ac) were higher in somatic follicle cells than in the germline (Fig. 5B; Supplemental Fig. S7C), suggesting that Enok levels are higher in follicle cells than in nurse cells. Therefore, high levels of Enok in somatic follicle cells seems to obscure the changes in Enok levels in the germline and result in a failure to detect reductions in Enok levels in the *enok RNAi* ovary by Western blotting (data not shown). To confirm the efficiency of RNAi against *enok* in nurse cells, we examined H3K23ac levels in ovaries by immunostaining. As shown in Figure 5B and Supplemental Figure S7C, the H3K23ac levels in nurse cells (white arrowheads) were decreased in *enok RNAi* and double RNAi ovaries as compared with *Luciferase* and *elg1 RNAi* ovaries, respectively, suggesting that the MTD-Gal4 driven RNAi against *enok* efficiently depleted Enok in nurse cells.

We next compared the morphology of nurse cell nuclei between *elg1 RNAi* and double RNAi ovaries. Although still underreplicated, nurse cell nuclei in the double RNAi ovary are relatively bigger and apparently have higher DNA content than those in the *elg1 RNAi* ovary (Fig. 5B; Supplemental Fig. S8A). In addition, in the double RNAi ovary with the *enok RNAi3* transgene, egg chambers in ~25% of the ovarioles were able to develop beyond stage 9 with morphologically normal nurse cells (Fig. 5B, bottom panel).

We further analyzed the cellular DNA content in these ovaries by flow cytometry (Fig. 5C; Supplemental Figs. S8B, S9). The *enok RNAi2* transgene seemed to have weaker rescuing effects on the endoreplication defects in Elg1-depleted nurse cells than the *enok RNAi3* transgene (cf. the bottom panels of Fig. 5B and Supplemental Fig. S7C). Therefore, the flow cytometric analysis for the *enok RNAi2;elg1 RNAi* ovaries were done in biological triplicates to confirm the reproducibility of results (Supplemental Figs. S8B, S9). Since the ploidy levels of somatic follicle cells range from 2C to 32C (Calvi and Lilly 2004), we focused on the population of nurse cells with a ploidy level of 64C–1024C to avoid interference from follicle cells. As shown in the bottom panels of Figure 5C and Supplemental Figure S8B, the *Luciferase* control, *enok RNAi2*, and *enok RNAi3* ovaries clearly showed five peaks of cells with a ploidy level of 64C, 128C, 256C, 512C, and 1024C. Consistent with the defective endoreplication phenotype, *elg1 RNAi* ovaries lack cells with ploidy levels of 128C–1024C and showed a peak only at 64C. Notably, the double RNAi ovaries with the *enok RNAi2* transgene had a 64C peak greater than that observed in the *elg1 RNAi* ovaries (Supplemental Figs. S8B,S9, arrow) and showed a peak of cells with a 128C ploidy level (Supplemental Figs. S8B,S9, open arrowhead). More dramatically, the double RNAi ovaries with the *enok RNAi3* transgene showed five peaks at 64C, 128C, 256C, 512C, and 1024C (Fig. 5C). These results strongly suggest that knocking down *enok* partially rescued the endoreplication defects in Elg1-depleted nurse cells. Furthermore, RNAi against *enok* also partially rescued the development of *elg1 RNAi* egg chambers. At stage 14, *Luciferase* and *enok RNAi* egg chambers showed fully developed dorsal appendages, while the dorsal appendages were lacking in the *elg1 RNAi* egg chambers (Supplemental Fig. S8C). However, the double RNAi egg chambers showed partially developed dorsal appendages (Supplemental Fig. S8C). Taken together, we concluded that *enok* genetically interacts with *elg1* in nurse cell endoreplication and oogenesis, supporting our hypothesis that Enok plays a negative role in regulating the PCNA-unloading function of the Elg1 complex.

Discussion

We report here that Enok forms a complex homologous to the human MOZ complex and that all four subunits contribute to its HAT function in vivo (Fig. 1). Notably, in addition to stimulating the HAT activity of Enok toward H3K23, Br140 also expanded its substrate specificity to include H3K14 in vitro (Fig. 1D; Huang et al. 2014). This result suggests that Br140 plays a role in regulating the enzymatic specificity of the Enok complex, which is consistent with the recent study showing that the human homolog of Br140, BRPF1, switches the substrate specificity of the HBO1 HAT complex to histone H3 (Lalonde et al. 2013). However, although BRPF1 interacts with both MOZ and HBO1 in human cells, we did not detect the *Drosophila* homolog of HBO1, Chameau, in Br140

purification, indicating that Br140 may be an Enok complex-specific component in flies.

Our study has also revealed a novel physical and functional interaction between the Enok HAT complex and the Elg1 PCNA-unloader complex, suggesting a role for Enok in modulating PCNA levels on chromatin during cell cycle progression (Figs. 2–5). The physical interaction between Enok and Elg1 complexes is also supported by a recent large-scale study on protein–protein interactions (Rhee et al. 2014). This study reported the interacting partners of 459 *Drosophila* transcription-related factors, and four subunits of the Elg1 complex (Elg1, Rfc4, Rfc38, and Rfc3) were identified by affinity purification using Br140 as the bait. Interestingly, instead of Elg1, the largest component of the PCNA-loader complex (Rfc1) copurified with the yeast Sas3-containing NuA3 complex using Pdp3 as the bait protein (Vicente-Munoz et al. 2014). This difference in interacting partners between the Enok and Sas3 complexes may be one of the reasons that Enok-depleted S2 cells accumulate at the G1 phase but that populations with a ploidy ≥2C (G2/M) accumulate when *SAS3* is deleted in *gcn5*Δ yeast cells (Howe et al. 2001). These results also raise the possibility that the roles of KAT6 HATs in regulating PCNA levels on the chromatin may be evolutionarily adapted by switching their interacting partners between different RFC/RFC-like complexes. The human MOZ complex has been implicated in playing a role in DNA replication via interacting with the MCM helicase and has been shown to regulate cell cycle arrest at the G1 phase by promoting p21 expression (Doyon et al. 2006; Rokudai et al. 2009). Given that MOZ is a critical regulator of proliferation of hematopoietic precursors and is involved in leukemia (Perez-Campo et al. 2009), it may advance our knowledge of hematopoiesis to investigate whether the MOZ complex also interacts with an RFC/RFC-like complex and regulates PCNA loading/unloading.

Reducing *enok* expression levels by dsRNA increased the rate of G2/M progression (Supplemental Fig. S4). While this faster G2/M progression is not dependent on Elg1, we also detected an ∼40% increase in the mRNA levels of the *Drosophila* CDC25 phosphatase that activates the mitotic kinase Cdk1, *string* (*stg*), in Enok-depleted cells (data not shown). As we reported previously that Enok plays a positive role in transcriptional activation by acetylating H3K23 (Huang et al. 2014), Enok may promote transcription of some repressor genes that down-regulate *stg* expression. Alternatively, Enok might repress transcription at a subset of gene loci, including *stg*, in a context-dependent manner, and, last, we cannot exclude the possibility that Enok may directly interact with other protein machinery to regulate G2/M progression.

Depletion of Enok also resulted in a block at the G1/S transition that is partially dependent on Elg1 (Fig. 3). This partial Elg1 dependence indicates that Enok has other roles in regulating the G1/S transition. While it is conceivable that Enok may regulate the expression of genes involved in cell cycle regulation, we did not detect significant changes in the mRNA levels of *Cyclin A*, *Cyclin B*, *Cyclin D*, *Cyclin E*, *Cyclin G*, *Cdk2*, *E2f1*, *Rbf*

(*Rb*), *dap* (*p21/p27*), *Dp*, or *Myc* in Enok-depleted S2 cells as compared with cells treated with control LacZ dsRNA (data not shown). Nevertheless, further genome-wide analysis of gene expression levels in Enok-depleted cells may provide more information on the transcriptional roles of Enok in cell cycle regulation.

Our model proposes that the Enok complex interacts with Elg1 via Br140 and down-regulates the PCNA-unloading function of Elg1 (Fig. 4C). This hypothesis is supported by the findings that Br140 interacts with Elg1 in vivo and in vitro (Fig. 2A,C) and that knocking down *enok* decreased the PCNA levels on chromatin (Fig. 4A, B). The Elg1 dependence of the G1/S block in Enok-depleted S2 cells (Fig. 3D–F) and the genetic interaction between *enok* and *elg1* in germline cells (Fig. 5) also agree well with our model, further supporting the negative role of the Enok complex in regulating Elg1 activity. Interestingly, we often observed small decreases in the Elg1 protein levels in Enok-depleted S2 cells or germline cells compared with the controls (Figs. 2B, 3C; Supplemental Figs. S5D, S7B), while the *elg1* mRNA levels remained largely unaffected by Enok depletion (Fig. 3E). This observation suggests that, in addition to regulating the PCNA-unloading function of the Elg1 complex, Enok may be involved in maintaining Elg1 protein levels or that the protein level and the PCNA-unloading activity of Elg1 may be inversely coregulated. Taken together, the physical and functional interactions between Enok and Elg1 provide a novel insight into the mechanisms underlying regulation of cell proliferation by KAT6 HATs.

Materials and methods

Fly strains and culture

Drosophila melanogaster was crossed and grown on standard medium at 25°C unless stated otherwise. MTD-Gal4-driven RNAi was carried out at 29°C. Females were conditioned with wet yeast for 2–3 d before ovary dissection. Embryos were collected using standard apple juice plates with wet yeast.

The following fly lines were obtained from the Bloomington *Drosophila* Stock Center: *UAS-Luciferase* (stock no. 35788), *UAS-enok RNAi1* (stock no. 40917), *UAS-enok RNAi2* (stock no. 42941), *UAS-elg1 RNAi* (stock no. 51453), *elg1^MI08386* (stock no. 44956), *Df(3L)Exel6128* (stock no. 7607), and *MTD-GAL4* (stock no. 31777).

The *UAS-enok RNAi3* fly line, which contains the same *P{TRiP.HMS02165}* insertion as the *UAS-enok RNAi1* fly line in the *attP40* site, was made by Rainbow Transgenic Flies, Inc., using the pVALIUM20 vector according to Transgenic RNAi Project (TRiP) protocols (Ni et al. 2011).

Complex purification

S2 cells stably expressing Flag-tagged Enok, Br140, Eaf6, Ing5, or Elg1 were lysed in buffer A (10 mM HEPES at pH 7.5, 1.5 mM MgCl$_2$, 10 mM KCl, 1% NP-40, 1 mM DTT, 1 mM PMSF, 5 mM sodium butyrate, 5 mM NaF, 1 μg/mL pepstatin A, 1 μg/mL leupeptin, 1 μg/mL aprotinin), and nuclei were isolated by centrifugation at 3000*g* for 5 min at 4°C. The nuclei were extracted in buffer B (20 mM HEPES at pH 7.5, 1.5 mM MgCl$_2$, 420 mM NaCl, 25% glycerol, 0.2 mM EDTA, 0.1% Triton X-100, 1 mM

DTT, 1 mM PMSF, 5 mM sodium butyrate, 5 mM NaF, 1 µg/mL pepstatin A, 1 µg/mL leupeptin, 1 µg/mL aprotinin) for 30 min at 4°C. After centrifugation at 245,000*g* for 2 h at 4°C, supernatant was collected and diluted using buffer A to a final NaCl concentration of 300 mM. The diluted NEs were incubated with 100 µL of anti-Flag affinity resin (Sigma, A2220) for 3 h at 4°C. Following three washes with 20 mL of wash buffer (10 mM HEPES at pH 7.5, 1.5 mM MgCl$_2$, 300 mM NaCl, 10 mM KCl, 0.2% Triton X-100, 1 mM PMSF, 5 mM sodium butyrate, 5 mM NaF), the anti-Flag resin was eluted three times with 250 µL of elution buffer (10 mM HEPES at pH 7.5, 1.5 mM MgCl$_2$, 100 mM NaCl, 0.05% Triton X-100, 10% glycerol, 500 µg/mL triple Flag peptide, 5 mM sodium butyrate, 5 mM NaF, 1 µg/mL pepstatin A, 1 µg/mL leupeptin, 1 µg/mL aprotinin) for 1 h at 4°C. The eluates were treated with 0.1 U of benzonase (Sigma) for 30 min at 37°C and subjected to TCA precipitation followed by MudPIT analysis.

MudPIT analysis

The TCA-precipitated pellet from the samples was solubilized in 100 mM Tris-HCl (pH 8.5) and 8 M urea, and TCEP [Tris(2-carbxy-lethyl)-phosphine hydrochloride] (Pierce) and CAM (chloroaceta-mide) (Sigma) were added to a final concentration of 5 and 10 mM, respectively. The protein suspension was digested overnight at 37°C using endoproteinase Lys-C at 1:50 (w/w) (Roche). The sample was brought to a final concentration of 2 M urea and 2 mM CaCl$_2$ before performing a second overnight digestion at 37°C using Trypsin (Promega) at 1:100 (w/w). Formic acid (5% final) was added to stop the reactions. Peptide mixtures were loaded onto a 100-µm fused silica microcapillary column packed with 8 cm of reverse phase material (Aqua, Phenomenex) followed by 3 cm of 5-µm Strong Cation Exchange material (Partisphere SCX, Whatman) followed by 2 cm of 5-µm C18 reverse phase (McDo-nalda et al. 2002). Loaded microcapillary columns were placed in-line with linear ion trap mass spectrometers (LTQ, Thermo-Scientific) coupled with quaternary Agilent 1100 or 1200 series high-performance liquid chromatographies (HPLCs). A fully auto-mated 10-step chromatography run (for a total of 20 h) was carried out for each sample, as described previously (Florens and Wash-burn 2006), enabling dynamic exclusion for 120 sec. The tandem mass spectrometry data sets were searched using Sequest (Eng et al. 1994) against a database of 43,158 sequences, consisting of 27,779 *D. melanogaster* nonredundant proteins (downloaded from NCBI on February 20, 2013), 177 usual contaminants (such as human keratins, IgGs, and proteolytic enzymes), and, to esti-mate false discovery rates (FDRs), 121,402 randomized amino acid sequences derived from each nonredundant protein entry. Peptide/spectrum matches were sorted, selected, and compared using DTASelect/Contrast (Tabb et al. 2002). Combining all runs, proteins had to be detected by at least two spectra, leading to FDRs at the protein and spectral levels of 1.36% and 0.12%, respectively. To estimate relative protein levels, normalized spec-tral abundance factors (dNSAFs) were calculated for each detected protein, as described previously (Zhang et al. 2010).

Antibody production

The recombinant peptide encompassing residues 1813–2197 of Enok was purified from *Escherichia coli* and injected into rabbits following the 28 Day Mighty Quick protocol conducted by Pocono Rabbit Farm and Laboratory. For generating the α-Elg1 an-tibody, a recombinant peptide encompassing the first 400 resi-dues of Elg1 was purified from *E. coli* and injected into rabbits and guinea pigs following the 28 Day Mighty Quick protocol car-ried out by Pocono Rabbit Farm and Laboratory.

RNAi knockdown in S2 cells

dsRNA synthesis and dsRNA treatment of S2 cells were per-formed essentially as described previously (Huang et al. 2014). Af-ter dsRNA treatment, S2 cells were incubated with the dsRNA for 4–7 d at 25°C before being subjected to acid extraction of histone, RNA isolation, flow cytometric analysis, or cell fractionation.

RNA purification and RT-qPCR

RNA isolation and cDNA synthesis were carried out as described previously (Huang et al. 2014). qPCR was performed in triplicate for each sample, and the data were analyzed using the standard curve method. The expression levels of *rp49* were used as the nor-malization control.

Acid extraction of histones

S2 cells were first lysed in buffer A. The nuclei were isolated by centrifugation at 1500*g* for 3 min at 4°C, resuspended in 0.4 N of HCl, and incubated for 5 min on ice. After centrifugation at 20,000*g* for 5 min at 4°C, supernatants were collected and neu-tralized with 2 M Tris (0.2× vol). Protein concentration was meas-ured using Bio-Rad protein assay, and an equal amount of protein was subjected to Western blotting.

Western blot analysis

The following primary antibodies were used in Western blot anal-ysis: Enok guinea pig (1:2000) (Huang et al. 2014), Enok rabbit (1:1000), Elg1 guinea pig (1:1000), Elg1 rabbit (1:1000), H3K14ac (1:1000; Millipore, 07-353), H3K23sc (1:100,000; Millipore, 07-355), H3 (1:10,000; Abcam, ab1791), H4 (1:3000; Abcam, ab7311); PCNA (1:1000; BD Biosciences, 555566), β-Tubulin (1:5000; Developmental Studies Hybridoma Bank [DSHB], E7), Flag (1:5000; Sigma, A8592), HA (1:2000; Roche, 12013819001), and Lamin (1:3000; DSHB, ADL67.10).

Purification of recombinant proteins from insect cells and in vitro HAT assay

Full-length cDNA of *Br140* was cloned into vector pBacPAK8 or pBacPAK8 carrying an N-terminal His-Flag tag. Full-length cDNA of *elg1* was cloned into vector pBacPAK8 carrying an N-terminal double HA tag. Purification of the recombinant Enok and Br140 from Sf21 cells was performed as described previously (Huang et al. 2014).

Short oligonucleosomes were purified from HeLa cells as de-scribed previously (Utley et al. 1997). Reconstitution of recombi-nant nucleosomes and in vitro HAT assay were carried out essentially as described in the previous study (Huang et al. 2014). Briefly, nucleosomes were incubated with or without recombinant Enok and/or Br140 in HAT buffer (50 mM Tris-HCl at pH 8.0, 50 mM KCl, 100 µM EDTA, 10 mM sodium buty-rate, 5% glycerol, 1 mM DTT, 100 µg/mL BSA, 1 mM acetyl-CoA, 1 mM PMSF) for 2 h at 27°C. For autoradiography (Fig. 1C, bottom two panels), 0.4 µCi of ^{3}H-acetyl-CoA (PerkinElmer) instead of 1 mM acetyl-CoA was used in 20-µL reactions, with a final concen-tration of 100 µM. The reactions were then adjusted using 2× SDS sample buffer to a final concentration of 1× (62.5 mM Tris-HCl at pH 6.8, 10% glycerol, 2% SDS, 0.01% bromophenol blue, 143 mM β-mercaptoethanol) and heated for 6 min at 98°C followed by Western blotting or autoradiography.

Cell fractionation

To prepare whole-cell extracts (WCEs) from S2 cells, cells were lysed in 1× SDS sample buffer and heated for 6 min at 98°C. After centrifugation at 20,000g for 5 min, supernatants were collected as WCEs. The cytosol fraction from S2 cells was obtained by lysing cells in buffer A followed by centrifugation at 1500g for 3 min at 4°C to separate the cytosol fraction (supernatant) and the nuclei (pellet). The cytosol fraction was then adjusted using 6× SDS sample buffer to a final concentration of 1× and heated for 6 min at 98°C. For NE preparation, the nuclei were washed once with buffer A and then either resuspended in 1× SDS sample buffer and heated for 6 min at 98°C for Western blotting (Figs. 1B, 3C, 4A; Supplemental Fig. S1B) or extracted in buffer B for 20 min on ice (Fig. 2B; Supplemental Figs. S1A, S5D). After extraction in buffer B, nucleus mixtures were centrifuged at 20,000g for 5 min at 4°C, and the supernatants were collected as NEs. The NEs were either subjected to co-IP (Fig. 2B) or adjusted using 6× SDS sample buffer to a final concentration of 1× and heated for 6 min at 98°C followed by Western blotting (Supplemental Figs. S1A, S5D). In Supplemental Figure S5D, after buffer B extraction and centrifugation, the chromatin pellets were resuspended in 1× SDS sample buffer, heated for 6 min at 98°C, and subjected to Western blotting as the chromatin fraction. In Supplemental Figures S2A and 4A, the chromatin fractions were prepared by lysing nuclei in hypotonic buffer (5 mM HEPES at pH 7.5, 3 mM EDTA, 200 µM EGTA, 1 mM DTT, 1 mM PMSF, 5 mM sodium butyrate, 5 mM NaF, 1 µg/mL pepstatin A, 1 µg/mL leupeptin, 1 µg/mL aprotinin) followed by centrifugation at 1700g for 3 min at 4°C. The chromatin pellets were washed once with hypotonic buffer, resuspended in 1× SDS sample buffer, heated for 6 min at 98°C, and subjected to Western blotting as the chromatin fraction.

To prepare WCEs from dechorionated embryos or ovaries, embryos or ovaries were homogenized in 1× SDS sample buffer and heated for 6 min at 98°C. After centrifugation at 20,000g for 5 min, supernatants were collected as WCEs. The chromatin-enriched fractions were obtained by homogenizing dechorionated embryos, larvae, or ovaries in buffer A followed by centrifugation at 1500g for 3 min at 4°C. The nuclei/chromatin pellets were washed once with buffer A and resuspended in 1× SDS sample buffer. Chromatin-enriched fractions were heated for 6 min at 98°C and then subjected to Western blot analysis. The NEs in Supplemental Figure S6A were prepared by extracting the nuclei/chromatin pellets from ovaries in buffer B for 30 min on ice followed by centrifugation at 20,000g for 10 min at 4°C. The supernatants were adjusted using 6× SDS sample buffer to a final concentration of 1×, heated for 6 min at 98°C, and subjected to Western blotting as NEs.

Co-IP assay

NEs from S2 cells were adjusted using buffer A to a final NaCl concentration of 200 mM (binding buffer) and incubated with rabbit preimmune serum, α-Enok, or α-Elg1 antiserum (1:50) for 16 h at 4°C. Protein A-conjugated Dynabeads (Novex) were added to the mixture and incubated for 1.5 h at 4°C. Beads were washed three times with binding buffer, heated in 1× SDS sample buffer for 6 min at 98°C, and subjected to Western blotting using guinea pig α-Enok or α-Elg1 antiserum.

Pull-down assay

The Sf21 cells expressing recombinant double HA-tagged Elg1 (2xHA-Elg1), His-Flag-Br140, His-Flag-Enok and/or no-tag Br140 were lysed in lysis buffer (50 mM HEPES at pH 7.5, 2 mM MgCl$_2$, 300 mM NaCl, 10% glycerol, 0.5 mM EDTA, 0.2% Triton X-100,

1 mM PMSF, 1 µg/mL pepstatin A, 1 µg/mL leupeptin, 1 µg/mL aprotinin) for 20 min on ice. After centrifugation at 20,000g for 10 min at 4°C, supernatants were collected and incubated with anti-Flag affinity resin or anti-HA affinity resin (Sigma, E6779) for 3 h at 4°C. Following three washes with lysis buffer, resins were heated in 1× SDS sample buffer for 6 min at 98°C and subjected to Western blot analysis.

Immunofluorescent staining

Ovaries were dissected in Shields and Sang M3 insect medium and processed as described previously (Shcherbata et al. 2004). For BrdU staining, ovaries were dissected and labeled with 10 µM BrdU for 1 h in Shields and Sang M3 insect medium. After two washes with the M3 insect medium, ovaries were fixed in 1× PBS containing 5% formaldehyde for 20 min. Ovaries were then washed three times with PBST (1× PBS containing 0.2% Triton X-100) and incubated in 2 N of HCl for 30 min followed by neutralization in 100 mM borax. After three washes with PBST, ovaries were subjected to a standard staining process with primary and secondary antibodies.

The following primary antibodies were used: γH2Av (1:100; Novus Biologicals, NBP1-78103), BrdU (1:20; BD Biosciences, 555627), and H3K23ac (1:2500; Millipore, 07-355). The following secondary antibodies were used: Alexa 568 goat anti-mouse (1:300; Molecular Probes) and Cy3 donkey anti-rabbit (1:300; Jackson ImmunoResearch). Cell nuclei were stained using 1 µg/mL DAPI dye (Invitrogen). Images were taken with a Zeiss LSM 510 confocal microscope or Leica SP5 X confocal microscope and processed using OMERO or ImageJ. Adobe Photoshop was used to assemble images into figures.

Flow cytometric analysis

For cell cycle profile analysis, S2 cells were washed once with 1× PBS and fixed in ice-cold 70% ethanol. After rehydration in 1× PBS, cells were incubated in 1× PBS containing 100 µg/mL RNase A (Qiagen) and 50 µg/mL propidium iodide (Invitrogen) for 30 min at 37°C and subjected to flow cytometric analysis of DNA content using MACSQuant (Miltenyi Biotec).

To analyze the progression of BrdU-positive cells during cell cycle, S2 cells were pulse-labeled with 15 µM BrdU for 15 min and released into BrdU-free medium for the time periods indicated in the figures. Cells were fixed in ice-cold 70% ethanol and then rehydrated in 1× PBS containing 0.5% BSA and 0.02% Tween 20 (PBS-BT) for 2 min. Following centrifugation at 1000g for 2 min at 4°C, cells were resuspended and incubated in 2 N of HCl for 30 min and then neutralized in 100 mM borax for 2 min. Cells were washed once with PBS-BT and incubated with α-BrdU (1:150) in PBS-BT for 30 min. After one wash with PBS-BT, cells were incubated with Alexa 488 goat anti-mouse (1:200; Molecular Probes) in PBS-BT for 30 min. Cells were then washed once with PBS-BT and incubated in 1× PBS containing 100 µg/mL RNase A and 50 µg/mL propidium iodide for 30 min at 37°C followed by biparametric BrdU/DNA analysis using MACSQuant or FACSCalibur (BD Biosciences).

Flow cytometric analysis of cellular DNA content in ovaries was performed as described previously using 35 pairs of ovaries for each sample (Huang et al. 2014).

Acknowledgments

References

Bellaoui M, Chang M, Ou J, Xu H, Boone C, Brown GW. 2003. Elg1 forms an alternative RFC complex important for DNA replication and genome integrity. *EMBO J* **22:** 4304–4313.

Ben-Aroya S, Koren A, Liefshitz B, Steinlauf R, Kupiec M. 2003. ELG1, a yeast gene required for genome stability, forms a complex related to replication factor C. *Proc Natl Acad Sci* **100:** 9906–9911.

Calvi BR, Lilly MA. 2004. Fluorescent BrdU labeling and nuclear flow sorting of the *Drosophila* ovary. *Methods Mol Biol* **247:** 203–213.

Doyon Y, Cayrou C, Ullah M, Landry AJ, Cote V, Selleck W, Lane WS, Tan S, Yang XJ, Cote J. 2006. ING tumor suppressor proteins are critical regulators of chromatin acetylation required for genome expression and perpetuation. *Mol Cell* **21:** 51–64.

Eng JK, McCormack AL, Yates JR. 1994. An approach to correlate tandem mass spectral data of peptides with amino acid sequences in a protein database. *J Am Soc Mass Spectrom* **5:** 976–989.

Florens L, Washburn MP. 2006. Proteomic analysis by multidimensional protein identification technology. *Methods Mol Biol* **328:** 159–175.

Garg P, Stith CM, Sabouri N, Johansson E, Burgers PM. 2004. Idling by DNA polymerase δ maintains a ligatable nick during lagging-strand DNA replication. *Genes Dev* **18:** 2764–2773.

Gilbert TM, McDaniel SL, Byrum SD, Cades JA, Dancy BC, Wade H, Tackett AJ, Strahl BD, Taverna SD. 2014. A PWWP domain-containing protein targets the NuA3 acetyltransferase complex via histone H3 lysine 36 trimethylation to coordinate transcriptional elongation at coding regions. *Mol Cell Proteomics* **13:** 2883–2895.

Hayashi R, Wainwright SM, Liddell SJ, Pinchin SM, Horswell S, Ish-Horowicz D. 2014. A genetic screen based on in vivo RNA imaging reveals centrosome-independent mechanisms for localizing gurken transcripts in *Drosophila*. *G3 (Bethesda)* **4:** 749–760.

Hong A, Narbonne-Reveau K, Riesgo-Escovar J, Fu H, Aladjem MI, Lilly MA. 2007. The cyclin-dependent kinase inhibitor Dacapo promotes replication licensing during *Drosophila* endocycles. *EMBO J* **26:** 2071–2082.

Howe L, Auston D, Grant P, John S, Cook RG, Workman JL, Pillus L. 2001. Histone H3 specific acetyltransferases are essential for cell cycle progression. *Genes Dev* **15:** 3144–3154.

Huang F, Paulson A, Dutta A, Venkatesh S, Smolle M, Abmayr SM, Workman JL. 2014. Histone acetyltransferase Enok regulates oocyte polarization by promoting expression of the actin nucleation factor spire. *Genes Dev* **28:** 2750–2763.

John S, Howe L, Tafrov ST, Grant PA, Sternglanz R, Workman JL. 2000. The something about silencing protein, Sas3, is the catalytic subunit of NuA3, a yTAF$_{II}$30-containing HAT complex that interacts with the Spt16 subunit of the yeast CP (Cdc68/Pob3)–FACT complex. *Genes Dev* **14:** 1196–1208.

Kanellis P, Agyei R, Durocher D. 2003. Elg1 forms an alternative PCNA-interacting RFC complex required to maintain genome stability. *Curr Biol* **13:** 1583–1595.

Kim J, MacNeill SA. 2003. Genome stability: a new member of the RFC family. *Curr Biol* **13:** R873–875.

Kubota T, Nishimura K, Kanemaki MT, Donaldson AD. 2013. The Elg1 replication factor C-like complex functions in PCNA unloading during DNA replication. *Mol Cell* **50:** 273–280.

Kubota T, Katou Y, Nakato R, Shirahige K, Donaldson AD. 2015. Replication-coupled PCNA unloading by the Elg1 complex occurs genome-wide and requires Okazaki fragment ligation. *Cell Rep* **12:** 774–787.

Lalonde ME, Avvakumov N, Glass KC, Joncas FH, Saksouk N, Holliday M, Paquet E, Yan K, Tong Q, Klein BJ, et al. 2013. Exchange of associated factors directs a switch in HBO1 acetyltransferase histone tail specificity. *Genes Dev* **27:** 2009–2024.

Lee KY, Yang K, Cohn MA, Sikdar N, D'Andrea AD, Myung K. 2010. Human ELG1 regulates the level of ubiquitinated proliferating cell nuclear antigen (PCNA) through Its interactions with PCNA and USP1. *J Biol Chem* **285:** 10362–10369.

Lee KY, Fu H, Aladjem MI, Myung K. 2013. ATAD5 regulates the lifespan of DNA replication factories by modulating PCNA level on the chromatin. *J Cell Biol* **200:** 31–44.

Lilly MA, Spradling AC. 1996. The *Drosophila* endocycle is controlled by Cyclin E and lacks a checkpoint ensuring S-phase completion. *Genes Dev* **10:** 2514–2526.

MacAlpine DM, Rodriguez HK, Bell SP. 2004. Coordination of replication and transcription along a *Drosophila* chromosome. *Genes Dev* **18:** 3094–3105.

Majka J, Burgers PM. 2004. The PCNA–RFC families of DNA clamps and clamp loaders. *Prog Nucleic Acid Res Mol Biol* **78:** 227–260.

McDonalda WH, Ohib R, Miyamotob DT, Mitchison TJ, Yates Iii JR. 2002. Comparison of three directly coupled HPLC MS/MS strategies for identification of proteins from complex mixtures: single-dimension LC-MS/MS, 2-phase MudPIT, and 3-phase MudPIT. *Int J Mass Spectrom* **219:** 245–251.

Moldovan GL, Pfander B, Jentsch S. 2007. PCNA, the maestro of the replication fork. *Cell* **129:** 665–679.

Ni JQ, Zhou R, Czech B, Liu LP, Holderbaum L, Yang-Zhou D, Shim HS, Tao R, Handler D, Karpowicz P, et al. 2011. A genome-scale shRNA resource for transgenic RNAi in *Drosophila*. *Nat Methods* **8:** 405–407.

Parnas O, Zipin-Roitman A, Mazor Y, Liefshitz B, Ben-Aroya S, Kupiec M. 2009. The ELG1 clamp loader plays a role in sister chromatid cohesion. *PLoS One* **4:** e5497.

Perez-Campo FM, Borrow J, Kouskoff V, Lacaud G. 2009. The histone acetyl transferase activity of monocytic leukemia zinc finger is critical for the proliferation of hematopoietic precursors. *Blood* **113:** 4866–4874.

Rhee DY, Cho DY, Zhai B, Slattery M, Ma L, Mintseris J, Wong CY, White KP, Celniker SE, Przytycka TM, et al. 2014. Transcription factor networks in *Drosophila melanogaster*. *Cell Rep* **8:** 2031–2043.

Rokudai S, Aikawa Y, Tagata Y, Tsuchida N, Taya Y, Kitabayashi I. 2009. Monocytic leukemia zinc finger (MOZ) interacts with p53 to induce p21 expression and cell-cycle arrest. *J Biol Chem* **284:** 237–244.

Rokudai S, Laptenko O, Arnal SM, Taya Y, Kitabayashi I, Prives C. 2013. MOZ increases p53 acetylation and premature senescence through its complex formation with PML. *Proc Natl Acad Sci* **110:** 3895–3900.

Royzman I, Hayashi-Hagihara A, Dej KJ, Bosco G, Lee JY, Orr-Weaver TL. 2002. The E2F cell cycle regulator is required for *Drosophila* nurse cell DNA replication and apoptosis. *Mech Dev* **119:** 225–237.

Scott EK, Lee T, Luo L. 2001. enok encodes a *Drosophila* putative histone acetyltransferase required for mushroom body neuroblast proliferation. *Curr Biol* **11:** 99–104.

Shcherbata HR, Althauser C, Findley SD, Ruohola-Baker H. 2004. The mitotic-to-endocycle switch in *Drosophila* follicle cells is executed by Notch-dependent regulation of G1/S, G2/M and M/G1 cell-cycle transitions. *Development* **131:** 3169–3181.

Sikdar N, Banerjee S, Lee KY, Wincovitch S, Pak E, Nakanishi K, Jasin M, Dutra A, Myung K. 2009. DNA damage responses by human ELG1 in S phase are important to maintain genomic integrity. *Cell Cycle* **8:** 3199–3207.

Tabb DL, McDonald WH, Yates JR III. 2002. DTASelect and Contrast: tools for assembling and comparing protein identifications from shotgun proteomics. *J Proteome Res* **1:** 21–26.

Taverna SD, Ilin S, Rogers RS, Tanny JC, Lavender H, Li H, Baker L, Boyle J, Blair LP, Chait BT, et al. 2006. Yng1 PHD finger binding to H3 trimethylated at K4 promotes NuA3 HAT activity at K14 of H3 and transcription at a subset of targeted ORFs. *Mol Cell* **24:** 785–796.

Ullah M, Pelletier N, Xiao L, Zhao SP, Wang K, Degerny C, Tahmasebi S, Cayrou C, Doyon Y, Goh SL, et al. 2008. Molecular architecture of quartet MOZ/MORF histone acetyltransferase complexes. *Mol Cell Biol* **28:** 6828–6843.

Utley RT, Cote J, Owen-Hughes T, Workman JL. 1997. SWI/SNF stimulates the formation of disparate activator-nucleosome complexes but is partially redundant with cooperative binding. *J Biol Chem* **272:** 12642–12649.

Venken KJ, Schulze KL, Haelterman NA, Pan H, He Y, Evans-Holm M, Carlson JW, Levis RW, Spradling AC, Hoskins RA, et al. 2011. MiMIC: a highly versatile transposon insertion resource for engineering *Drosophila melanogaster* genes. *Nat Methods* **8:** 737–743.

Vicente-Munoz S, Romero P, Magraner-Pardo L, Martinez-Jimenez CP, Tordera V, Pamblanco M. 2014. Comprehensive analysis of interacting proteins and genome-wide location studies of the Sas3-dependent NuA3 histone acetyltransferase complex. *FEBS Open Bio* **4:** 996–1006.

Yang XJ, Ullah M. 2007. MOZ and MORF, two large MYSTic HATs in normal and cancer stem cells. *Oncogene* **26:** 5408–5419.

Zhang Y, Wen Z, Washburn MP, Florens L. 2010. Refinements to label free proteome quantitation: how to deal with peptides shared by multiple proteins. *Anal Chem* **82:** 2272–2281.